Describing the spatio-temporal variability of vines and soil by satellite-based spectral indices: A case study in Apulia (South Italy)

Describing the spatio-temporal variability of vines and soil by satellite-based spectral indices: a case study in Apulia (South Italy)

E. Borgogno-Mondino[1,a], V. Novello[1], A. Lessio[1], L. de Palma[2]

[1]Department of Agricultural, Forest and Food Sciences, University of Turin, Italy; [2]Department of the Sciences of Agriculture, Food and Environment, University of Foggia, Italy

Abstract

A time series of Landsat 8 OLI (L8 OLI) multispectral images acquired between May 2013 and February 2016 were used to investigate vigour, vine and soil water content in a vineyard of Moscato Reale (syn. Moscato Bianco) sited in the Castel del Monte DOCG area. Normalized difference vegetation index (NDVI) and normalized difference water index (NDWI) were calculated and compared with vine midday stem water potential (Ψ_{MDstem}) and soil volume water content (VWC), to calibrate estimation models. Estimation models were calibrated using already existing ground observation datasets from previous ordinary vineyard management operations: Ψ_{MDstem} was measured at two different locations in vineyard at 6 different dates in summer 2014; VWC was continuously measured from June to October 2014 and from January to September 2015. Results showed that: a) vine stem water potential can be locally estimated with an accuracy ranging from ±0.046 (high vigour vines) to ±0.127 (low vigour vines) MPa; b) soil volume water content can be locally estimated with an accuracy of about ±1.7%. Medium resolution satellite imagery proved, therefore, to be effective, at vineyard level, to describe vigour, vine and soil water status and their seasonality. This is an important issue to focus on since, as Landsat 8 images are free, the entire process is economic enough to be consistent with cost and incoming of the farming system.

[a] E-mail: enrico.borgogno@unito.it

Keywords: NDVI, NDWI, vine midday stem water potential, soil volume water content, Landsat 8 OLI

1. INTRODUCTION

Monitoring crop water status in vineyard is essential to optimize water supply and has a significant impact on agriculture sustainability, especially in semi-arid Mediterranean regions. In wine grape production, plant water status is widely recognized as a critical factor for attaining and maintaining a high quality level, since it exerts a direct effect on berry growth, grape yield, skin structure, metabolite concentration and, especially under particular climate conditions, on flavonoid biosynthesis (Ojeda at al., 2002; Roby et al, 2004). Nonetheless, it affects also photosynthate export and partitioning among organs, shoot vigour and bunch microclimate, and exerts an indirect effect on grape composition and wine sensorial attributes (Bota et al. 2004; Chaves et al., 2007).

Crop water status is known to change in space and time, depending on soil properties and moisture, root development, canopy vigour, topography, irrigation uniformity and several other factors. Geomatics techniques have proved to be a helpful tool in supporting agronomical practices and are more and more entering the production workflow (Bonilla et al., 2015). In particular, optical remote sensing permits vegetation monitoring in space and time; in the last decades, it demonstrated to be effective in describing some plants biophysical features, such as vigour, that can be related to fruit/wine quality and potential yield (Hall et al., 2011; Ledderhof et al., 2016). Unmanned Aerial Vehicles (UAVs) are the newest and, probably, the most used remote sensing technology in precision farming. Unfortunately, in spite of many reported experiences (Torres-Sanchez et al., 2014; Candiago et al., 2015), data provided by low cost sensors from UAV are still affected by some critical issues (scene radiometric consistency, spectral features of bands, reliability of information, etc…) that, currently, have not been completely explored (Borgogno-Mondino, 2017).

Furthermore, UAVs, at the moment, due to their limited operational endurance, can be only thought to operate over small areas. Borgogno-Mondino & Gajetti (2017) showed that, in the Italian context, UAV acquisition costs are consistent with the low incomes of the agriculture sector (lower than 10 €/ha) only if imaged areas for single flight is greater than about 50 ha, moving toward a spatial scale that reasonably is more consistent with aerial and satellite imagery. Additionally, satellite and aerial images are generally more reliable since: a) detailed technical specifications for sensors are available, b) the entire vineyard usually falls into a single scene making pixels homogeneous from a radiometric point of view. Due to high performance of sensors and chance to acquire images at a specific time without limitations due to cloud coverage, aerial data are probably the best solution to monitor crops, but also the most expensive choice (Matese et al. 2015). Differently, in spite of their low geometric resolution, consistent with many applications at vineyard/field level, satellite data present some peculiar features: they are free, recurrent in time (Bramley et al. 2003) and benefit of sensor having a generally higher spectral resolution. In particular, those sensors can acquire bands belonging to an important range of the spectrum that is mostly missing in ordinary aerial multispectral sensors: the medium infrared region (1.0-2.5 microns). The NASA (National American Space Agency) Landsat 8 and ESA (European Space Agency) Sentinel I-II datasets (Malenovský et al., 2012; Frampton et al., 2013) can be considered the reference products for this type of application. These products can certainly play an important role in precision farming, both at regional and single-field/vineyard level. Some works have already proved the correlation between satellite data and some biophysical parameters (Johnson et al., 2003), as well as their efficiency to monitor vigour of vegetated surfaces (Testa et al., 2014). Moreover, since they are made available for free, they are economically consistent with the costs and incomings of farming systems (Borgogno-Mondino et al., 2017).

In spite of a wide literature concerning the utilization of satellite-derived spectral indices to get estimates of biophysical parameters of vines and soil properties by regressive models, the following questions still persist: a) can reliable estimates of ground measures be obtained using models

calibrated on not perfectly overlaying (especially in time) satellite images and ground observations?; b) does the accuracy of estimates depend on plant or soil status?

This work aims to give some preliminary answers to these questions, well knowing that all results have to be intended as specific for the investigated vineyard and that no general conclusion can be given.

Focusing on a vineyard sited in Southern Italy, spectral indices from Landsat 8 (L8) operational land imager (OLI) data were related to vine water status (Acevedo-Opazo, 2008), as stem water potential (Ψ_{MDstem}), and to soil moisture, as volume water content (VWC). In particular, NDVI (Normalized Difference Vegetation Index, Rouse et al., 1974) and NDWI (Normalized Difference Water Index, Gao, 1996) time series were generated and related to the available ground measures. Assuming NDVI and NDWI as proxies of Ψ_{MDstem} and VWC respectively, correspondent relationships were modelled and uncertainty of estimates measured.

Authors acknowledge that the experimental design of ground data is not perfectly responding to a rigorous scientific approach: in fact, ground measures and satellite images are not perfectly aligned in time, and ground data are very few both in time and space. Nevertheless, they present a crucial peculiarity: they were already available and free from past ordinary vineyard management practices of farmers. The exploitation of previously existing measures, that someone collected in the past for different goals, is desirable to make technology transfer easier and consistent with the costs of the agriculture sector.

2. MATERIALS AND METHODS

2.1 Test area, satellite and ground measures datasets

A vineyard of Moscato Reale (syn. Moscato Bianco), sizing about 37000 m^2, centred around 611895 E, 4548884 N coordinates (UTM 33N WGS84 reference frame) and located in Apulia (SE Italy) was selected as test area. The vineyard belongs to the DOC zone of Castel del Monte (Figure 1).

100 Basing on the climatic dataset of Apulia Region Government, and according to the classification of
101 Rivas-Martínez et al. (1999), this zone proves to have a "Mediterranean pluviseasonal-oceanic
102 semicontinental" bioclimate, characterized by alternation of favourable/limiting periods for plant
103 growth.

104

105 [FIGURE 1]

106

107 Twenty-five Landsat 8 OLI/TIRS images, Level-2 Data Products - Surface Reflectance, (table 1)
108 with a spatial resolution of 30 m, were obtained from the EarthExplorer web system
109 (http://earthexplorer.usgs.gov/) covering the period 19/05/2013 – 05/0272016 (hereinafter called
110 reference period). The vineyard was imaged by 37 L8 OLI pixels.
111 Measures of soil VWC (%) were available, from past vineyard management operations, at two
112 positions, respectively representative of averagely higher (V+) and lower (V-) vigour (Figure 1b,
113 white dots). They were obtained by sensors of dielectric constant positioned at 35-40 cm depth
114 (Decagon's ECH2O 5TM) and automatically collected, at 15' step, from June to October 2014 and
115 from January to September 2015. At the same positions, measures of vine midday stem water
116 potential (Ψ_{MDstem}, MPa) were available too, but covering a shorter time range (June-August 2014).
117 Measurements were obtained by a Scholander pressure bomb (Soil Moisture Corp., Santa Barbara,
118 CA, USA), according to McCutchan and Shakel (1992). Per each position, measurements were
119 taken on a group of 10 vines surrounding the soil VWC sensor; ten readings per position were
120 collected to represent the local vineyard behaviour. In this work, Ψ_{MDstem} is expressed in terms of
121 absolute values. It is worth to remind that measurements of both VWC and Ψ_{MDstem} were not fitting
122 the date nor the hour of satellite acquisitions, being available from previous campaigns.

123

2.2 Data processing

NDVI and NDWI were computed according to equations (2) and (3):

$$NDVI = \frac{\rho_{NIR} - \rho_{RED}}{\rho_{NIR} + \rho_{RED}} \quad (2)$$

$$NDWI = \frac{\rho_{NIR} - \rho_{SWIR1}}{\rho_{NIR} + \rho_{SWIR1}} \quad (3)$$

where ρ_{RED}, ρ_{NIR} and ρ_{SWIR1} are the at-the-ground reflectance in band 4 (0.630–0.680 μm), band 5 (0.845–0.885 μm) and band 6 (1.560–1.660 μm), respectively.

Since ground and satellite dataset were not timely consistent, a chronological aligning step was achieved. An estimation of both NDVI and NDWI from satellite imagery at the same days of ground ones was given by interpolating observed values along a 1-day-stepped time series. Regularization was achieved at pixel level by considering all available NDVI/NDWI values, corresponding to 25 sampling dates irregularly spaced in time, and calibrating a cubic spline with tension = 5 (De Boor et al., 1978) for a period of 992 days (about 3 years) to approximate the whole temporal profile of pixel. A daily estimation of NDVI and NDWI was thus given, even included that corresponding to ground measurements

2.3 Vineyard vigour mapping

Previous research experiences in the same test area (de Palma et al., 2016) showed that, in the vineyard, high vigour portions (V+) alternate with low vigour ones (V-). As above mentioned, ground measures were taken at 2 locations representing V+ and V-, respectively. According to this a-priori knowledge, the vineyard was mapped in two clusters (Figure 2) to separate V+ from V- zones. An automatic classification (iterative minimum distance - Forgy, 1965) was achieved based on the average NDVI value $\mu_{NDVI}(x,y)$, computed by eq. (4) for each pixel in the reference period (interpolated NDVI time series).

147 $$\mu_{NDVI}(x^*, y^*) = \frac{\sum_{t=1}^{992} NDVI_t(x^*, y^*)}{992} \quad (4)$$

148 where $\mu_{NDVI}(x^*, y^*)$ is the average value of NDVI of the generic pixel located at (x^*, y^*) in the
149 vineyard, and $NDVI_t(x^*, y^*)$ the value of NDVI at the same position recorded at the *t* date; 992 is
150 the number of days for which an estimate of NDVI was known after daily interpolation of the
151 original data. All tests and calibrations were performed separately for V+ and V- pixels.

152

153 **2.4 Minimizing vegetation effects in NDWI**

154 An intermediate step was needed at this point; in fact, due to the coarse geometric resolution of the
155 L8 OLI sensor, vineyard pixels, necessarily include both soil (corridors) and vegetation (vines).
156 Since NDWI is intended for VWC detection of the soil fraction, vegetation effects must be
157 minimized. For this task, scatterplots relating NDVI and NDWI (Figure 3) were generated showing
158 a strong correlation. Aside the main trend of the modelled regression, a de-correlated information
159 persists in model residuals computed according to eq. (5). They were assumed as proxies of soil
160 VWC.

161 $$NDWI' = NDWI - (a \cdot NDVI + b) \quad (5)$$

162 where *a* and *b* are the coefficients of the linear regression relating NDWI to NDVI.

163

164 **2.5 Relating ground measures to spectral indices**

165 For the available dates, and separately for V+ and V- classes (table 1), ground measures of Ψ_{MDstem}
166 and soil VWC were respectively compared with NDVI and NDWI' through the following ratios:

167 $$R1 = \frac{\Psi_{MDstem}}{NDVI} \quad (6)$$

168 $$R2 = \frac{VWC}{(NDWI' + 0.1)} \quad (7)$$

The term (+0.1) in eq. (7) was introduced to make positive original NDWI' values, thus possible applying the power model. All models depend on vine vigour class, giving significantly different values for V+ and V- observations.

R1 definition was reached by relating, separately, NDVI and Ψ_{MDstem} to DOY (Day of the Year). A strong correlation was observed and a 2nd order polynomial function used to model relationships (Figure 5 a, b).

$$\begin{cases} \mathrm{NDVI} = k_0 t^2 + k_1 t + k_2 & (a) \\ \Psi_{\mathrm{MDstem}} = h_0 t^2 + h_1 t + h_2 & (b) \end{cases} \quad (8)$$

where k_0, k_1, k_2 and h_0, h_1, h_2 are the coefficient values estimated by an ordinary least squares (OLS) estimation process.

Combining both models along a numerical system, eq. (8), the following general equation was obtained:

$$\Psi_{\mathrm{MDstem}} = R1(t) \cdot NDVI \quad (9)$$

where *R1(t)* is, rigorously, a ratio between two independent 2nd order polynomial functions of time.

Inverting eq. (9) and plotting computed values of $R1(t) = \frac{\Psi_{\mathrm{MDstem}}}{NDVI}$ in respect of DOY, it can be observed that both V+ and V- are well fitted by a 2nd order polynomial, eq. (10), whose parameters are significantly different for the two classes.

$$R1(t) = a_0 t^2 + a_1 t + a_2 \quad (10)$$

where a_0, a_1, a_2 are the coefficient values estimated by OLS and *t* the date of observations as DOY.

Differently, an exponential function proved to well fit the relationship between *R2* and NDWI':

$$R2 = b_1 e^{b_2 NDWI'} \quad (11)$$

where b_1 and b_2 are the coefficient values estimated by OLS.

To test the effect of including NDVI in Ψ_{MDstem} estimation, some concerns were done about both model parameters stability/robustness and uncertainty of estimates.

Being the available ground datasets too small (not properly adequate) a leave-one-out (LOO) cross-validation approach was adopted (Picard & Cook, 1984). Since LOO generate different estimates of model parameters at each iteration (n. of iterations = n. of ground observations), the final parameter estimate was computed like the average value (μ_{a_i}) of all its values. Stability of estimates was measured by the standard error ($\frac{\sigma_{a_i}}{\sqrt{n}}$). To make more evident uncertainty of parameter estimates the coefficient of variation ($CV = \frac{\sigma_{a_i}}{\mu_{a_i}} \cdot 100$) was computed too (Table 5).

MAE (Mean Absolute Error, eq. (12)) was assumed as measure of estimate accuracy (or uncertainty).

$$MAE = \frac{\sum_{i=1}^{N} |x_{obs} - x_{est}|_i}{N} \quad (12)$$

where $|x_{obs} - x_{est}|$ is the absolute value of the difference between the measured value and its estimate.

With the only goal of pointing out the role that such a modelling could have within an operational context, two pairs of maps of Ψ_{MDstem} and VWC at two arbitrary dates (2nd July 2014 and 2015), within the explored period, were generated.

3. RESULTS AND DISCUSSIONS

Twenty-five L8 OLI images, 11 VWC and 6 Ψ_{MDstem} measures, obtained at two positions in vineyard (V+ and V-), were used. Values and accuracy of ground measures are reported in Table 1, together with dates of acquisition of L8 OLI images.

Table 1. Ground measure of soil VWC and vine Ψ_{MDstem}. V+ and V- represent the high and low vigour sample points in vineyard, respectively (see Figure 1b). Dates of L8 OLI image acquisitions are reported in the last two columns.

Date	V+ VWC (%)	V- VWC (%)	Date	V+ Ψ_{MDstem}(MPa)	V– Ψ_{MDstem}(MPa)	Date of L8 OLI image acquisition	
23/06/2014	14.52 ±1.61	21.35 ±1.91	*02/06/2014*	0.544 ±0.018	0.404 ±0.056	19/05/2013	26/08/2014
09/07/2014	12.74 ± 1.42	24.90 ± 1.87	*23/06/2014*	0.460 ±0.018	0.492 ±0.027	20/06/2013	13/10/2014
10/08/2014	9.89 ± 1.23	22.99 ± 1.86	*28/06/2014*	0.643 ±0.019	0.745 ±0.021	06/07/2013	17/01/2015
26/08/2014	9.98 ± 1.21	24.18 ± 1.76	*02/08/2014*	0.625 ±0.099	0.602 ±0.044	07/08/2013	18/02/2015
13/10/2014	9.79 ± 1.34	18.59 ± 1.71	*23/08/2014*	0.920 ±0.043	1.222 ± 0.030	10/10/2013	10/06/2015
17/01/2015	17.30 ± 1.51	7.36 ± 1.12	*08/09/2014*	1.552 ±0.026	1.676 ±0.041	14/01/2014	12/07/2015
18/02/2015	18.01 ± 1.86	8.49 ± 1.16				15/02/2014	28/07/2015
10/06/2015	13.70 ± 1.52	22.19 ± 1.87				19/03/2014	13/08/2015
12/07/2015	14.50 ± 1.48	23.69 ±1.89				22/05/2014	29/08/2015
28/07/2015	14.28 ± 1.56	24.87 ±1.93				23/06/2014	14/09/2015
13/08/2015	12.23 ± 1.32	24.14 ± 1.89				09/07/2014	03/12/2015
						10/08/2014	05/02/2016

3.1 Vineyard vigour mapping

Irregularly spaced time series of NDVI and NDWI were generated and interpolated by spline with tension (value of tension = 5) to get a daily estimations within the reference period.

The average NDVI value, along the correspondent time series, was computed for all the vineyard pixels. An unsupervised classification, with two classes, was performed to separate V+ and V- pixels. Observations outside vine growing season were not filtered out, for the following reasons: a) farmers reported that V+ an V- were mainly conditioned by local soil properties all along the year; b) mean value is representative of the total (cumulated) annual vigour; c) this strategy is not influenced by the spatial distribution of V+ and V- classes, that, differently, could heavily condition an approach based on local anomaly computation (difference, or ratio, between the local NDVI value and the vineyard average one).

Clustering showed that the two ground measurement stations fell into different classes (Figure 2), making possible the interpretation of their meaning. Statistics of clusters are reported in Table 2. This preliminary clustering step was mandatory to separate V+ from V- pixels and apply the proper model in the different part of vineyard.

[FIGURE 2]

Table 2. Statistics of NDVI and NDWI' for V+ and V- clusters (Iterative Minimum Distance algorithm).

Spectral Index	V-		V+	
	Mean	Std. Dev.	Mean	Std. Dev.
NDVI	0.39	0.03	0.49	0.02
NDWI'	0.017	0.013	0.007	0.012

3.2 Relating ground measures to spectral indices

NDVI and NDWI values of vineyard pixels (37) were graphed by scatterplot; a linear function was used to model the relationship. To minimize "vegetation effects" when using NDWI as proxy of VWC, the correlated information was removed from the original NDWI values according to eq. (15) assuming that regression residuals (hereinafter called NDWI') were better proxies of soil VWC.

$$NDWI' = NDWI - (0.7034 \cdot NDVI - 0.1647) \quad (15)$$

[FIGURE 3]

Consequently, correlations between satellite-derived indices and ground measures were tested. The following correlations were computed, separately, for the two vigour classes (V+ and V-): Ψ_{MDstem} vs. NDVI, Ψ_{MDstem} vs. NDWI', VWC vs. NDVI, VWC vs. NDWI' (Figure 4).

[FIGURE 4]

Table 4. Pearson's correlation coefficients (at p-value < 0.01), separately calculated for V+ and V-, between spectral indices and ground data of Ψ_{MDstem} and VWC.

Index	Cluster	Ψ_{MDstem}	VWC
NDVI	V+	0.32	0.36
	V-	0.05	0.59
NDWI'	V+	0.36	0.57
	V-	0.04	0.11

Strength of correlations and scatterplot cloud shapes proved that no regression model could generate accurate estimates of Ψ_{MDstem} and VWC by directly relating spectral index with ground measures.

R1 and R2 ratios were considered as possible alternatives; the following correlations were tested: R1 vs. DOY, R1 vs. NDVI and R2 vs. NDWI'. Since correlations were found to be strong ($R > 0.75$), relationships were modelled: R1 was related to DOY and to NDVI by a 2nd order polynomial. R2 was related to NDWI' by an exponential function. Pearson's correlation coefficients and model parameters, included standard error and coefficient of variation of model parameters estimates by LOO, are reported in Table 5.

[FIGURE 5]

[FIGURE 6]

Table 5 shows that Ψ_{MDstem} estimates obtained including NDVI are more robust (stable) than those obtained only considering DOY, even if correlation coefficient values are comparable. In fact, both SE and CV of model parameters estimated by LOO cross-validation are significantly lower in the first estimation approach for both V+ and V- classes.

Table 5. Parameters of calibrated models. SE= standard error; CV = coefficient of variation. Correlations are tested at p-value <0.01.

Class	a_0			a_1			a_2			R
	value	SE	CV (%)	value	SE	CV (%)	value	SE	CV (%)	
$R1 = a_0t^2 + a_1t + a_2$										
V+	0.00051	0.00002	4%	-0.18759	0.00746	4%	18.36732	0.67397	4%	0.802
V-	0.00100	0.00013	13%	-0.00746	0.05075	14%	36.46838	5.05053	14%	0.771
$\Psi_{MDstem} = a_0t^2 + a_1t + a_2$										
V+	0.00015	0.00002	13%	-0.05484	0.00784	14%	5.35292	0.76361	14%	0.848
V-	0.00014	0.00004	29%	-0.04606	0.01795	39%	4.32824	1.79622	42%	0.884
$R2 = a_0e^{a_1(NDWI'+0.1)}$										
V+	130.11616	0.24370	0.6%	-15.9413	0.10991	2.2%				-0.903
V-	125.69176	0.21619	0.5%	-9.00119	0.05489	1.9%				-0.787

It can be therefore said that Ψ_{MDstem} estimates by R1 (including NDVI information) is preferable, whatever is the uncertainty of estimates (Table 6). It is worth to point out that estimates of model parameters is significantly different for V+ and V- classes, making evident that this type of approach is very sensible to local environmental/soil conditions. Further developments have still to be done,

especially concerning stability of model coefficients in time (they could change in different growing seasons). Nevertheless these preliminary results are encouraging.

Table 6 shows estimate uncertainty (MAE) for both vine Ψ_{MDstem} and VWC given by calibrated models.

Table 6. Uncertainty of estimates. The mean absolute error (MAE) was assumed as measure of uncertainty. Table reports both mean and standard deviation of MAE as resulting from the iterations of the LOO cross-validation.

Predictor	MAE Ψ_{MDstem} [MPa]
NDVI V+	0.046 ± 0.007
NDVI V-	0.127 ± 0.016
Time (DOY) V+	0.086 ± 0.010
Time (DOY) V-	0.127 ± 0.016
	MAE Soil VWC [%]
NDVI V+	1.746 ± 0.075
NDVI V-	1.715 ± 0.042

According to Table 6 it can be stated that: a) Ψ_{MDstem} estimations are more accurate for V+ than for V- parts of vineyard; b) estimations from the model directly relating Ψ_{MDstem} and DOY are less accurate than those based on R1. The local NDVI value modulates the correspondent average Ψ_{MDstem} value of the day (as obtainable through DOY), making possible an intra-vineyard mapping of Ψ_{MDstem}, i.e. local variations of Ψ_{MDstem} around the cluster (V+ or V-) average trend.

Results also showed that the potential uncertainty affecting estimates was averagely 0.1 MPa for Ψ_{MDstem} (range of variation = 0.5-1.6 MPa) and about 1.7% for VWC (range of variation = 9-20 %). These values, in spite of the simplified approach and of the low quality of ground measures distribution in time and space, are consistent, and sometimes better, than the expected ones. Comparing uncertainty of estimates given by models with the one originally affecting ground measures (table 1) it can be noticed that: uncertainty of estimates of Ψ_{MDstem} is about 2-3 times

higher; uncertainty of estimates of VWC is completely consistent with the ground measured one. No specific reference perfectly fitting this work were found in literature. Nevertheless, Champagne et al. (2003) using, the Probe-1 airborne hyperspectral sensor, applying an extremely rigorous radiative transfer model for image calibration (MODTRAN4), and an opportune ground sampling strategy, could estimate EWT (equivalent water thickness, cm) for different crops (wheat, canola, corn, beans and peas) with an accuracy (root mean squared error, RMSE) of about 0.052 cm, for ground measures ranging between 0 and 0.3 cm (error > 20 %). Bellvert et al. (2014) explored the adoption of thermal infrared sensors to get estimates of Ψ_{MDstem}, but the focuse was on the strength and shape of correlation withno definitive value for estimates uncertainty.

Concerning the uncertainty of VWC, Jacome et al. (2013) estimated it by radar multi polarization data from RADARSAT-2 with an accuracy of 10 %: it was almost 5 time higher than the one given by the models proposed in this work.

3.3 Periodicity of spectral indices

With these premises, daily estimations of both Ψ_{MDstem} and VWC in the reference period were respectively generated by separate models for V+ and V- clusters. Daily estimates of Ψ_{MDstem} and VWC were computed at cluster level according to the V+ and V- average temporal profiles of NDVI and NDWI'. Some evident anomalies were found for Ψ_{MDstem} estimates (Figure 7a); out of the range values of Ψ_{MDstem} (up to 6 or 7 MPa) were obtained recurrently along years. Such values cannot be retained consistent with those expected for vines: midday stem water potential values higher than 1.4 MPa indicates severe water deficit (Van Leeuwen et al., 2009), values higher than 1.64 MPa are found in non-irrigated vines (Williams & Araujo, 2002), and a maximum of 1.8 MPa was found in the present trial. Ψ_{MDstem} estimates along the year were compared with an arbitrary, but reasonable, maximum admissible value of 2 MPa. Only within the vine growing season (from about April to October) estimates proved to be consistent with ground measured values and lower than 2 MPa. In

the same period, NDVI values showed a great variability proving that NDVI cannot be considered a robust proxy of Ψ_{MDstem} without taking care about the DOY of measurements.

[FIGURE 7]

Using the interpolated time series of NDWI' (averaged over V+ and V- classes), temporal profiles of soil VWC were estimated in the reference period (figure 8) through the calibrated model.

[FIGURE 8]

Graphs of figure 8 show that VWC tends to remain quite stable low along the year (about 12%) in V- parts of vineyard; differently, in V+ parts of vineyard, VWC changes from a minimum of about 10% up to about 35%. This has generally occurred in opposite to NDWI' profile, supporting the convincement that soil capacity to keep water conditions markedly vine vigour; once more, water supply management shows to be a delicate step for making vineyard behaviour more homogeneous. To translate these considerations into the practical agronomic management, two scenarios were generated by vine Ψ_{MDstem} and soil VWC respectively. An arbitrary date within the growing season of vines was selected for the simulation: maps of estimates of Ψ_{MDstem} and VWC were generated through the above mentioned models at the following dates: 2/07/2014 and 2/7/2015 (Figure 9).

[FIGURE 9]

Simulated scenarios (Figures 7, 8 and 9) are not intended to demonstrate consistency of estimates. They are just intended to make clear how model estimates can be accessed and represented in such a way that they can be easily interpreted by vineyard managers.

Class width was selected greater than the expected estimation uncertainty (0.1 MPa for Ψ_{MDstem} and 1.7% for VWC).

4. CONCLUSIONS

This work proved that multispectral medium resolution satellite imagery are effective in mapping vine and soil water status to support vineyard management. It also proved that existing ground measures, that do not perfectly fit scientific requirements in terms of repetitions and space distribution, can be effectively used to calibrate satellite-based models for vines and soil water content estimation if proper processing strategies (e.g. LOO approach) are adopted to minimize those limits. In these conditions, satellite-derived NDVI and NDWI' (de-trended NDWI) proved to be correlated to vine midday stem water potential and with soil volume water content, respectively. Models relating ground measures to spectral indices were found depending on vineyard vigour class (high or low), making clear that no general predictive model for both Ψ_{MDstem} and VWC can be imagined without an a-priori knowledge of vineyard spatial variability. It was also demonstrated that a model directly relating Ψ_{MDstem} to DOY, with no regard of NDVI, is less accurate and reliable than the one including NDVI; moreover NDVI local value can tune the daily estimation of Ψ_{MDstem}. Models can be successfully used to generate reliable estimations of vine Ψ_{MDstem} and soil VWC for whatever date when spectral indices are available.

Finally, supported by the obtained results, this work demonstrated that vineyard knowledge can be augmented by combining proper processing strategies such as free satellite data and ground measures obtained from past campaigns and/or from ordinary vineyard management practices. These ingredients are promising, especially for the agronomic sector where technology transfer has to be driven carefully, considering the related costs and their incidence on the farm financial balance.

5. ACKNOWLEDGEMENTS

The research was carried out with the financial support of MiUR and Regione Puglia, within PON02_00186_2866121 project.

The authors would like to thank TORRESANTA farm and TORREVENTO winery (Corato, Bari, Italy), and Dott. Luigi Tarricone (CREA-UTV, Turi-BA, Italy) for their valuable collaboration as project partners.

References

1. Acevedo-Opazo, C., Tisseyre, B., Guillaume, S., Ojeda, H. (2008). The potential of high spatial resolution information to define within-vineyard zones related to vine water status. Precision Agriculture, 9(5), 285-302.

2. Bellvert, J., Zarco-Tejada, P. J., Girona, J., & Fereres, E. (2014). Mapping crop water stress index in a 'Pinot-noir'vineyard: comparing ground measurements with thermal remote sensing imagery from an unmanned aerial vehicle. Precision agriculture, 15(4), 361-376.

3. Bonilla, I., Martinez de Toda, F., Martinez-Casanovas, A. (2015). Vine vigour, yield and grape quality assessment by airborne remote sensing over three years: Analysis of unexpected relationship in cv. Tempanillo. Spanish Journal of Agricultural Research, 13(2), 1-8.

4. Borgogno Mondino E. (2017) Remote Sensing from RPAS in Agriculture: An Overview of Expectations and Unanswered Questions. In: Ferraresi C., Quaglia G. (eds) Advances in Service and Industrial Robotics. RAAD 2017. Mechanisms and Machine Science, vol 49. Springer, Cham

5. Borgogno-Mondino, E., Gajetti, M. (2017). Preliminary considerations about costs and potential market of remote sensing from UAV in the Italian viticulture context. European Journal of Remote Sensing, 50(1), 310-319.

6. Borgogno-Mondino, E., Lessio, A., Tarricone, L., Novello, V., de Palma, L. (2017). A comparison between multispectral aerial and satellite imagery in precision viticulture. Precision Agriculture,(in press).

7. Bota, J., Stasyk, O, Flexas, J, Medrano, H. (2004). Effect of water stress on partitioning of 14C-labelled photosynthates in Vitisvinifera. Functional Plant Biology, 31, 697-708.

8. Bramley, R., Pearse, B., Chamberlain, P. (2003). Being Profitable Precisely – A case study of Precision Viticulture from Margaret River. Australian Grapegrower and Winemaker, 473a, 84–87.

9. Candiago, S., Remondino, F., De Giglio, M., Dubbini, M., Gattelli, M. (2015). Evaluating multispectral images and vegetation indices for precision farming applications from UAV images. Remote Sensing, 7(4), 4026-4047.

10. Champagne, Catherine M., et al. "Validation of a hyperspectral curve-fitting model for the estimation of plant water content of agricultural canopies." Remote Sensing of Environment 87.2 (2003): 148-160.

11. Chaves, M.M., Santos, T.P., Souza, C.R., Ortuño, M.F., Rodrigues, M.L., Lopes, C.M., Maroco, J.P., Pereira, J.S. (2007). Deficit irrigation in grapevine improves water-use efficiency while controlling vigour and production quality. Annals of Applied Biology, 150, 237–252.

12. De Boor, C., De Boor, C., Mathématicien, E. U., De Boor, C., De Boor, C. (1978). A practical guide to splines (Vol. 27, p. 325). New York: Springer-Verlag.

13. de Palma, L., Tarricone, L., Borgogno, E., Limosani, P., Paolicelli, M., Novello V. (2016). Fisiologia e qualità della produzione in Nero di Troia e Moscato Reale, in relazione alle differenze di vigore rilevate con tecniche di viticoltura di precisione. Acta Italus Hortus, 19, 177-178.

14. Forgy, E. (1965). Cluster Analysis of multivariate data: efficiency vs. interpretability of classifications'. Biometrics, 21, 768.

15. Frampton, W. J., Dash, J., Watmough, G., & Milton, E. J. (2013). Evaluating the capabilities of Sentinel-2 for quantitative estimation of biophysical variables in vegetation. ISPRS journal of photogrammetry and remote sensing, 82, 83-92.

16. Gao, B.C. (1996). NDWI – A normalized difference water index for remote sensing of vegetation liquid water from space. Remote Sensing of Environment, 58(3), 257-266.

17. Hall, A., Lamb, D.W., Holzapfel, B.P., Louis, J.P. (2011). Within-season temporal variation in correlations between vineyard canopy and winegrape composition and yield. Precision Agriculture, 12(1), 103-117.

18. Jacome, A., Bernier, M., Chokmani, K., Gauthier, Y., Poulin, J., & De Sève, D. (2013). Monitoring volumetric surface soil moisture content at the La Grande basin boreal wetland by radar multi polarization data. Remote Sensing, 5(10), 4919-4941.

19. Johnson, L.F., Roczen, D.E., Youkhana, S.K., Nemani, R.R., Bosch, D.F. (2003). Mapping vineyard leaf area with multispectral satellite imagery. Computers and Electronics in Agriculture, 38(1), 33-44.

20. Ledderhof, D., Brown, R., Reynolds, A., Jollineau, M. (2016). Using remote sensing to understand Pinot noir vineyard variability in Ontario. Canadian Journal of Plant Science, 96(1), 89-108.

21. Malenovský, Z., Rott, H., Cihlar, J., Schaepman, M. E., García-Santos, G., Fernandes, R., & Berger, M. (2012). Sentinels for science: Potential of Sentinel-1,-2, and-3 missions for scientific observations of ocean, cryosphere, and land. Remote Sensing of environment, 120, 91-101.

22. Matese, A., Toscano, P., Di Gennaro, S. F., Genesio, L., Vaccari, F. P., Primicerio, J., ... & Gioli, B. (2015). Intercomparison of UAV, aircraft and satellite remote sensing platforms for precision viticulture. Remote Sensing, 7(3), 2971-2990.

23. McCutchan, H, Shackel, K.A. (1992). Stem-water Potential as a Sensitive Indicator of Water Stress in Prune Trees (Prunusdomestica L. cv. French). Journal of the American Society for Horticultural Science. 117(4), 607-611.

24. Ojeda, H., Andary, C., Kraeva, E., Carbonneau, A., Deloire, A. (2002). Influence of pre and postveraison water deficit on synthesis and concentration of skin phenolic compounds during berry growth of Vitisvinifera cv Shiraz. American Journal of Enology and Viticulture, 53, 261–267.

25. Picard, R., Cook, D. (1984). Cross-Validation of Regression Models. Journal of the American Statistical Association. 79 (387): 575–583. doi:10.2307/2288403.

26. Rivas-Martínez, S., Sanchez-Mata, D., Costa, M., (1999). North American boreal and western temperate forest vegetation (syntaxonomical synopsis of North America, II). Itinera Geobotanica, 12, 5-316.

27. Roby, G., Harbertson, J.F., Adams, D.O., Matthews, M.A. (2004). Berry size and vine water deficits as factors in winegrape composition: Anthocyanins and tannins. Australian Journal of Grape and Wine Research, 10, 100-107.

28. Rouse JW, Haas RH, Schell JA, Deering DW (1974). Monitoring vegetation systems in the Great Plains with ERTS, Third ERTS Symposium, NASA SP-351 I, pp. 309-317.

29. Testa, S., Borgogno-Mondino, E., Pedroli, C. (2014). Correcting MODIS 16-day composite NDVI time-series with actual acquisition dates. European Journal of Remote Sensing, 47, 285-305.

30. Torres-Sánchez, J., Peña, J. M., De Castro, A. I., & López-Granados, F. (2014). Multi-temporal mapping of the vegetation fraction in early-season wheat fields using images from UAV. Computers and Electronics in Agriculture, 103, 104-113.

493
494 31. Van Leeuwen C., Tregoa O., Choné X., Bois B., Pernet D., Gaudillère J.-P. (2009). Vine water status is a key
495 factor in grape ripening and vintage quality for red Bordeaux wine. How can it be assessed for vineyard
496 management purposes? Journal International des Sciences de la Vigne et du Vin, 43(3), 121-134
497
498 32. Williams, L.E., Araujo, F.J (2002). Correlations among predawn leaf, midday leaf and midday stem water
499 potentials and their correlations with other measures of soil and plant water status in Vitisvinifera.
500 Journal of the American Society for Horticultural Science, 127(3), 448-454.
501

FIGURES CAPTIONS

Figure 1. (a) Test area location in Apulia (Italy). (b) Aerial view of the vineyard. White dots correspond to ground measurements stations.

Figure 2. Map showing V+ (high vigour) and V- (low vigour) parts of vineyard. Classification was achieved by clustering vineyard pixels in respect of their average NDVI value in the reference period (19/05/2013-05/02/2016). To be noticed that ground sampling stations are placed in a different cluster, confirming that they are representative of two different states of the vineyard (high and low vigour).

Figure 3. (a) NDWI vs. NDVI before trend removal. (b) NDWI' vs. NDVI after trend removal.

Figure 4. Scatterplots directly relating ground measures to spectral indices. The following scatterplots were generated (and correspondent Pearson's Coefficient computed, Table 4) separately for V+ (high vigour) and V- (low vigour): Ψ_{MDstem} vs. NDVI, Ψ_{MDstem} vs. NDWI', VWC vs. NDVI, VWC vs. NDWI' (Ψ_{MDstem} is expressed in terms of absolute values).

Figure 5. Scatterplots relating: (a) NDVI vs. DOY; (b) Ψ_{MDstem} vs. DOY; (c) R1 vs. DOY. Relationships were modelled, separately for V+ (continuous line) and V- (dotted line), by a 2^{nd} order polynomial.

Figure 6. Scatterplots relating: (a) NDWI' vs. DOY; (b) VWC and DOY; (c) R2 and NDWI'. The latter relationship was modelled, separately, for V+ (continuous line) and V- (dotted line), by an exponential model.

Figure 7. (a) Average profiles of NDVI (interpolated series) and Ψ_{MDstem} as estimated by models. Bold line traits of NDVI profiles indicate where Ψ_{MDstem} estimates are lower than the selected threshold, while grey rectangles define the time range where they occurred. (b) Differences between Ψ_{MDstem} estimates obtained, respectively, by eq. (7b) and (9). Graph only reports differences within the previously defined growing seasons (Ψ_{MDstem} is expressed in terms of absolute values).

Figure 8. Temporal profiles of soil VWC estimates in the reference period ((19/05/2013-05/02/2016)) estimated by model using the interpolated time series of NDWI'. Estimates are given separately for V+ and V- classes.

Figure 9. Example showing maps of estimates of Ψ_{MDstem} *(expressed in terms of absolute values) and VWC obtained by models. Estimates refer to July 2nd 2014 (a, b) and July 2nd 2015 (c, d). Mapped classes bins of* Ψ_{MDstem} *and VWC have a width of 0.1 MPa and 1.5%, respectively, according to the uncertainty of estimates from models.*

541 Figure 1

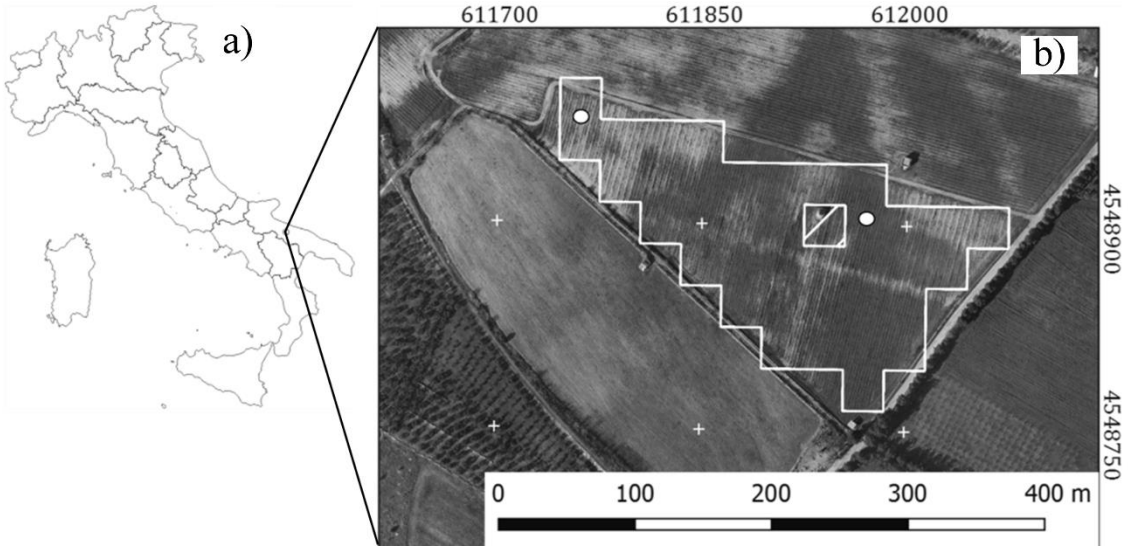

542

543

544 Figure 2

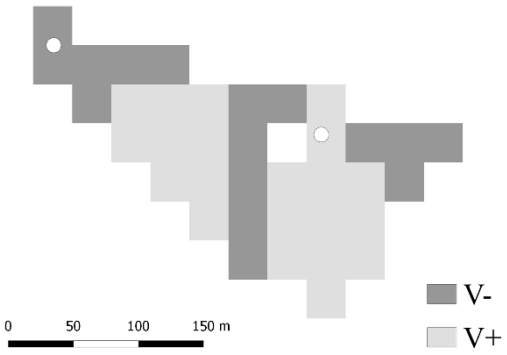

545

546 Figure 3

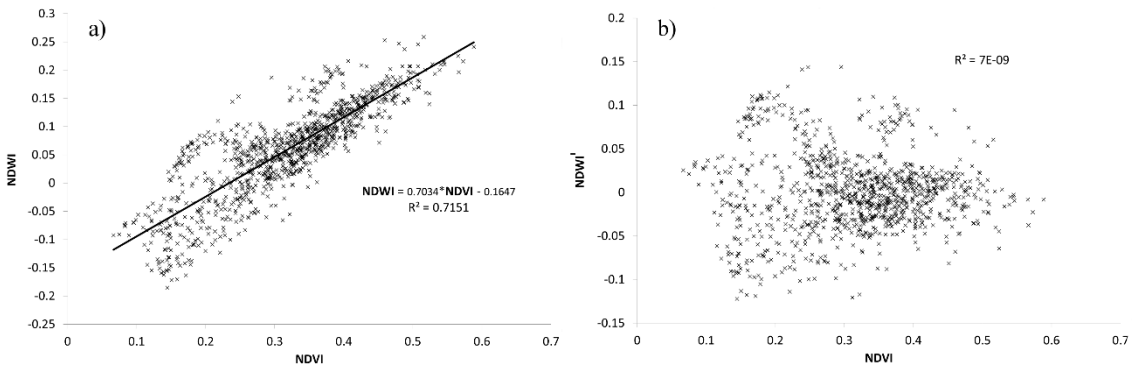

547

548

549

Figure 4

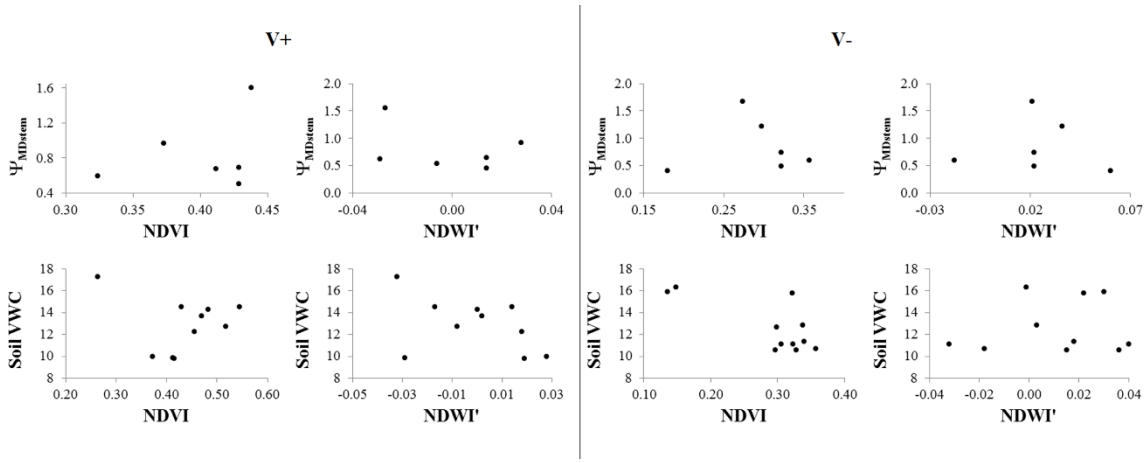

Figure 5

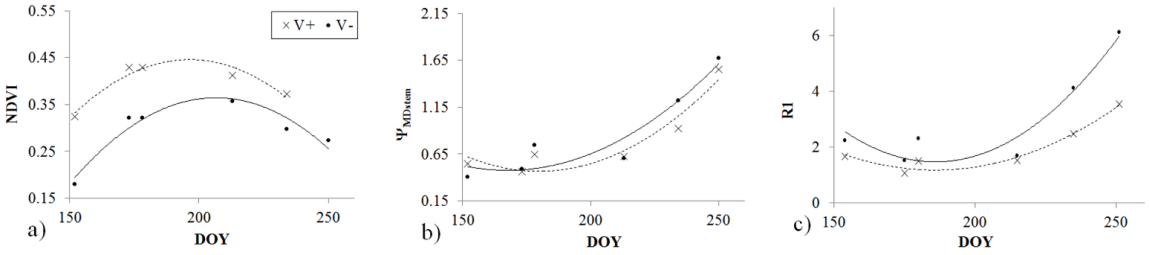

Figure 6

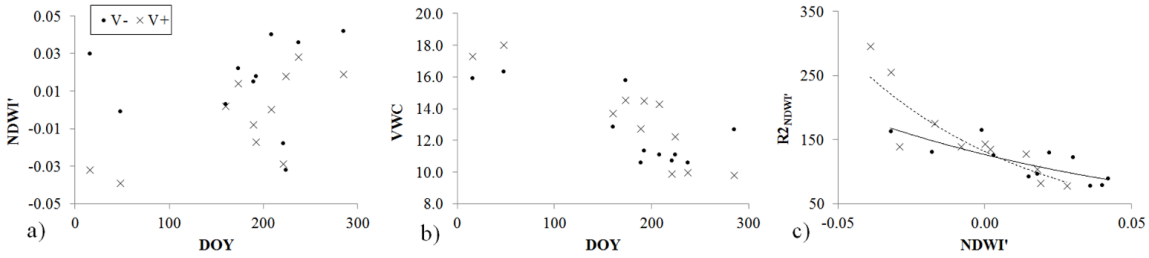

Figure 7

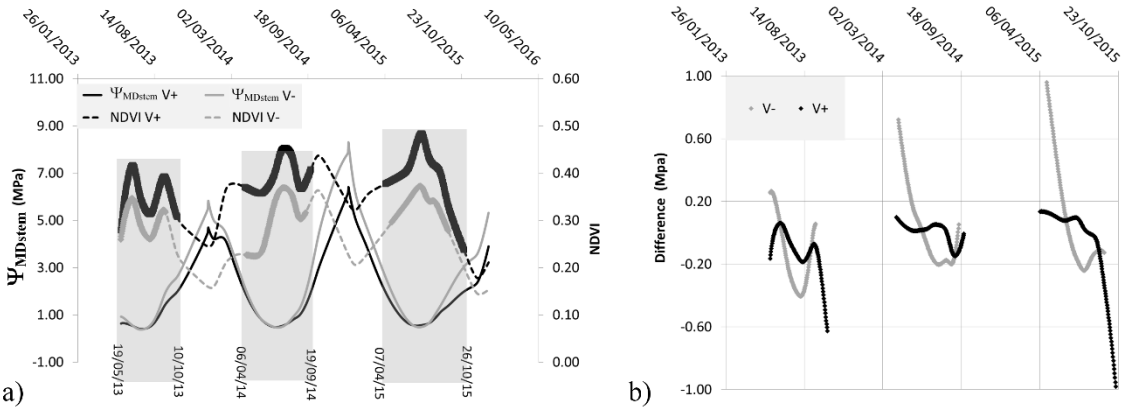

558 Figure 8

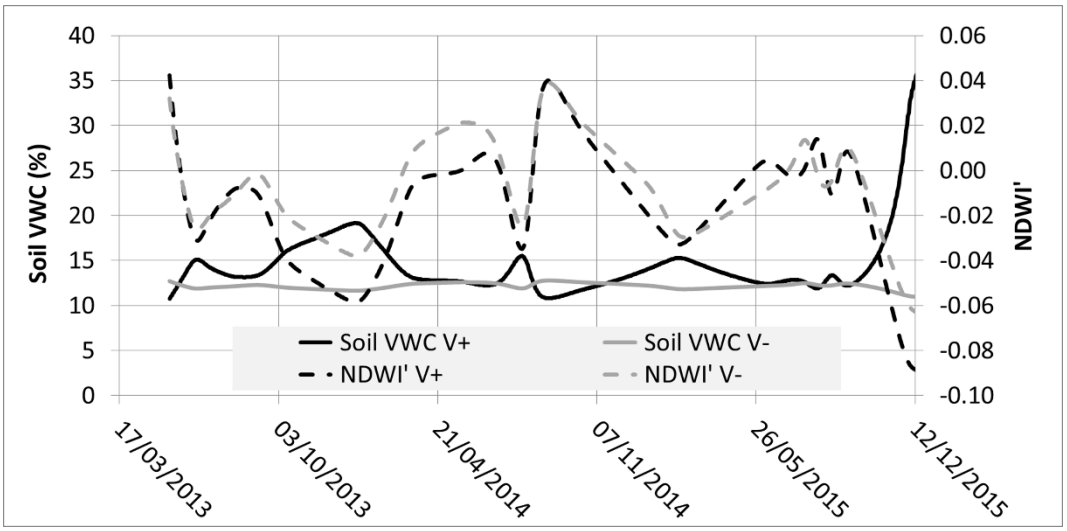

559

560

561 Figure 9

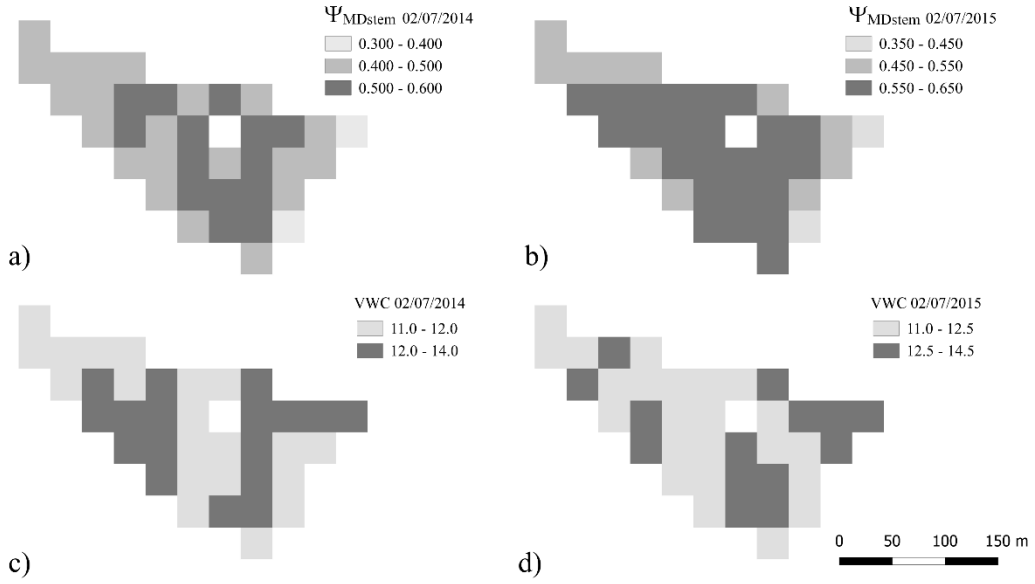

562

563

564

565